Applied Surface Science 447 (2018) 599–609

Contents lists available at ScienceDirect

Applied Surface Science

journal homepage: www.elsevier.com/locate/apsusc

Full Length Article

An experimental study on soft PDMS materials for aircraft icing mitigation

Yang Liu [a], Liqun Ma [a], Wei Wang [b], Arun K. Kota [b], Hui Hu [a,*]

[a] Department of Aerospace Engineering, Iowa State University, 2271 Howe Hall, Room 1200, Ames, IA 50011, USA
[b] Department of Mechanical Engineering, Colorado State University, Fort Collins, CO 80523, USA

ARTICLE INFO

Article history:
Received 11 February 2018
Revised 16 March 2018
Accepted 4 April 2018
Available online 5 April 2018

Keywords:
Soft PDMS materials
Dynamics of droplet impingement
Ultra-low ice adhesion material
Impact icing process
Aircraft icing mitigation

ABSTRACT

A series of experiments were conducted to characterize the anti-/de-icing performances of soft PDMS materials with different shear modulus and to explore their potentials for aircraft icing mitigation. In the present study, a new class of soft PDMS materials with adjustable shear modulus were fabricated by adding different amounts and different molecular weights of non-reactive trimethyl-terminated PDMS (t-PDMS) into the hydrosilylation mixture of vinyl-terminated PDMS (v-PDMS) and hydride-terminated PDMS (h-PDMS). While the soft PDMS materials were found to be hydrophobic with the contact angle of water droplets over the PDMS surfaces being about 110°, the ice adhesion strength over the soft PDMS materials was found to be extremely low (i.e., being less than 10 kPa at −5 °C or two orders of magnitude smaller), in comparison to those of the conventional rigid surface (i.e., being greater than 1000 kPa for Aluminum or the hard plastic material used to make the airfoil/wing model used in the present study). Upon the dynamic impacting of water droplets at relatively high weber number levels pertinent to aircraft inflight icing phenomena (e.g., *We* = 4000), the soft PDMS surfaces were found to deform dynamically due to the elastic nature of the PDMS materials, which cause the soft PDMS materials acting as "trampolines" to bounce off most of the impinged water mass away from the impacted surfaces. By applying the soft PDMS materials to coat/cover the surface of a NACA 0012 airfoil/wing model, an exploratory study was also performed in an Icing Research Tunnel available at Iowa State University (i.e., ISU-IRT) to demonstrate the feasibility of using the soft PDMS materials to mitigate the impact ice accretion process pertinent to aircraft inflight icing phenomena.

1. Introduction

Aircraft icing is widely recognized as one of the most serious weather hazards to aircraft operation. Airplanes flying in cold weathers conducive to ice accretion must be equipped with anti-/de-icing mechanisms; otherwise, flight delays, cancellations and abortions may occur because of the forecast or actual in-flight icing. While significant research progress has been made in recent years for an improved understanding about aircraft icing phenomena [1–8], aircraft icing remains an important unsolved problem at the top of the National Transportation Safety Board's most wanted list of aviation safety improvements.

While a number of anti-/de-icing systems have already been developed and implemented for aircraft icing mitigation, current anti-/de-icing strategies suffer from various drawbacks. For example, aqueous solutions of propylene and ethylene glycol along with other chemical additives are widely used for aircraft anti-/de-icing at airports, which has been an increasing concern of the environmental impacts from the aircraft anti-/de-icing fluid swept away with storm and melt water runoff at airports to ground water and nearby waterways [9]. Pneumatic de-icing systems with rubber boots have been used to break off large ice chunks accreted at airfoil leading edge for aircraft in-flight icing mitigation, but they are usually very heavy and sometimes unreliable [10]. Ultrasonic and mechanical de-icing solutions are not easily integrated into existing aircraft and pose foreign object damage (FOD) hazards to aero-engines [10,11]. While electro-thermal de-icing systems have been used to melt out ice by heating aircraft wing surfaces, they are usually very inefficient and have demanding power requirements, and can also cause damage to composite materials from overheating. Furthermore, the melted water from the thermally protected regimes may simply run back and re-freeze at downstream locations to cause uncontrolled ice accretion [10].

Specialized hydro- and ice-phobic coatings/materials are currently being investigated for use as viable strategies to mitigate

* Corresponding author.
E-mail address: huhui@iastate.edu (H. Hu).

https://doi.org/10.1016/j.apsusc.2018.04.032
0169-4332/

ice accretion on aircraft [12–17]. Inspired by the outstanding self-cleaning capability of lotus leaves and duck feathers, a number of studies have been conducted in recent years to develop coatings to make super-hydrophobic surfaces, on which water droplets bead up with a very large contact angle (i.e., >150°) and drip off rapidly when the surface is slightly inclined [18–23]. One attractive application of the super-hydrophobic surfaces, in addition to the extraordinary water-repellency, is their potential to reduce accumulation of snow and ice over solid surfaces. Under a frost-free environment (e.g., low humidity conditions), some super-hydrophobic surfaces were found to show promising behaviors in delaying ice formation [13,24] even at temperatures as low as −25 to −30 °C [25]. While most of those coatings have undergone simple and static tests (i.e., by spraying water droplets or pouring water onto substrates, and then froze the test samples in refrigerators) to demonstrate the hydro- and ice-phobic characteristics for anti-frosting applications [26,27], their capabilities to mitigate *impact icing* process pertinent to aircraft in-flight icing phenomena have been under debate for several years [28–31]. Here, the concept of "*impact icing*" is defined as ice formed due to the dynamic collision of macroscopic super-cooled water droplets onto a surface at a high impact velocity. The structure of impact icing can vary considerably depending upon the conditions in which the ice is formed. Air temperature, air speed, water droplet size, liquid water content, and airframe geometry would all affect the ice structure that accretes.

It is well known that almost all super-hydrophobic surfaces are textured or rough surfaces [32–37]. As shown schematically in Fig. 1, when a water droplet comes in contact with a textured super-hydrophobic surface, it adopts the so-called *Cassie-Baxter state* [37–39] with air trapped in the surface textures beneath the droplet. Since the water droplet is supported by the air pocket, it beads up and displays very high contact angles (typically >150°). However, under icing conditions, water can condense from the surrounding humid air within the surface textures to form the so-called *Wenzel state* [40], with water completely wetting the pores or asperities of the textures. Furthermore, for the aircraft in-flight icing scenario, super-cooled water droplets would impact onto textured surfaces at high speeds and readily penetrate into the surface textures (i.e., transition from the Cassie-Baster state to the fully wetted Wenzel state) [40], resulting in completely wetting the pores or asperities of the textures. Once the water is frozen within the textures in the *Wenzel state*, it would be extremely difficult to remove the ice, even more difficult than on non-textured surfaces, because of the interlocking between ice and the textures [41,42]. Consequently, some super-hydrophobic surfaces were found to display higher ice adhesion strengths, in comparison to non-textured surfaces, substantially increasing the amount of energy required to remove the accumulated ice [36,43–45]. In summary, super-hydrophobicity with textured surface does not necessarily imply icephobicity, especially for the aircraft in-flight icing scenario with high-speed impacts of super-cooled water droplets onto the wing surfaces.

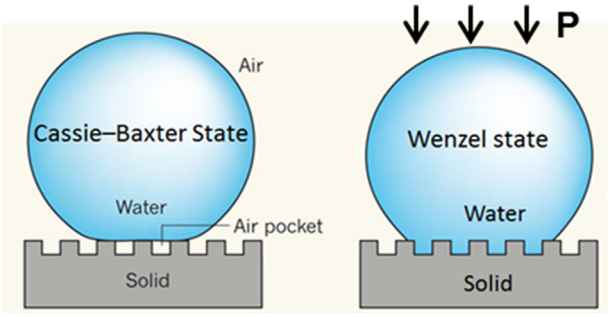

Fig. 1. Schematic of a water droplet on a textured surface in either the Cassie or the Wenzel states.

Another strategy to reduce ice adhesion strength onto a solid surface is to use a layer of liquid lubricant, which is immiscible with water, between ice and the solid surface. The use of such lubricated surfaces was investigated as early as 1960s [46–49], and has gained increasing attentions again recently with the introduction of Slippery Liquid-Infused Porous Surfaces (SLIPS) [50–52]. Replacing the ice-solid interface with highly deformable ice-lubricant and solid-liquid interfaces induces slipperiness between ice and the solid. Consequently, SLIPS were found to display very low ice adhesion strength typically on the order of a few kPa [50,53]. Such low ice adhesion strength is highly desirable because it will facilitate easy removal of the accreted ice over the solid surface. One concern about SLIPS for anti-/de-icing applications is the sacrificial nature of the liquid lubricant: the infused liquid could eventually be depleted by evaporation at elevated temperature or at reduced pressure [54]. As ice slides past the lubricated surface, a portion of the liquid lubricant may also be shaved off by the accreted ice, demoting the longevity of the lubricated materials [55]. It should be noted that, a novel self-lubricating liquid water layer (SLWL) based anti-icing coating has been developed recently to address this concern by employing hydrophilic polymers to lock a thin layer of water on the solid surface to act as the lubricant [56,57]. Since the water can be supplied by ice continuously, there will be no concern over the depletion of the lubricant [57]. Another concern is the durability of the SLIPS upon mechanical contact, which can potentially damage the substrate and deplete the infused liquid, degrading the mechanical integrity of the surface [54].

More recently, soft materials/surfaces, which would be structurally deformed/altered dynamically by applying extra mechanical stress, were also been suggested for icing mitigation. For example, a recent study of Beemer et al. [55] demonstrated that, soft materials of polydimethylsiloxane (PDMS) gels have ultra-low ice adhesion strength as well as good mechanical durability. The PDMS gels display ultra-low adhesion to ice due to their low work of adhesion and liquid-like deformability, while maintaining good mechanical durability due to their solid-like rigidity. This can be better explained by invoking classical adhesion mechanics. According to classical adhesion mechanics postulated by Griffith [58] and further elaborated by Kendall [59] and Chaudhury & Kim [60], the lower work of adhesion, lower shear modulus, and larger thickness of the surface material would lead to lower ice adhesion strength. Hydrophobic gels possess ultra-low adhesion to ice because hydrophobic materials typically possess low work of adhesion and gels typically possess a low shear modulus. Furthermore, unlike lubricated materials, hydrophobic gels possess a better mechanical durability because of their adhesive failure, instead of sacrificial (i.e., cohesive) failure [55]. Building on these principles, hydrophobic PDMS materials/gels were designed with low cross-link density and correspondingly low shear modulus that offer ultra-low adhesion to ice as well as good mechanical durability (virtually unlimited icing/de-icing cycles and up to 1000 abrasion cycles with no obvious change in ice adhesion strength) [55]. It should also be noted that, the PDMS materials/gels are transparent with an optical transmittance of more than 90% in the visible range [61]. The unique characteristics of the soft PDMS materials evokes our interests to conduct the present study to explore the potentials of using soft PDMS materials for aircraft icing mitigation.

In the present study, soft PDMS materials with adjustable shear modulus are fabricated by adding different concentrations of non-reactive trimethyl-terminated PDMS (t-PDMS) into the hydrosilylation mixture of vinyl-terminated PDMS (v-PDMS) and hydride-terminated PDMS (h-PDMS). A series of experiments are

conducted to characterize the material properties of the soft PDMS materials in terms of static contact angles, dynamic contact angles of water droplets, and ice adhesion strength over the PDMS surfaces at different frozen temperatures. The impinging dynamics of water droplets onto the soft PDMS surfaces is also examined by using a high-speed imaging system, in comparison with the case with water droplets impinging onto a conventional rigid surface, in order to examine the influence of the surface stiffness on the impinging dynamics of the water droplets at relatively high weber numbers pertinent to aircraft inflight icing phenomena. By applying the soft PDMS materials to coat/cover the surface of a NACA 0012 airfoil/wing model, an explorative study is performed in a unique Icing Research Tunnel available at Iowa State University (i.e., ISU-IRT in short) to demonstrate the feasibility of using the soft PDMS surface/-materials to mitigate impact icing process pertinent to aircraft inflight icing phenomena.

2. Preparation of soft PDMS materials/surfaces and experimental setup

2.1. Preparation of soft PDMS materials/surfaces with tunable shear modulus

In the present study, soft PDMS materials/surfaces with different shear modulus were fabricated via hydrosilylation of vinyl-terminated PDMS (v-PDMS) with hydride-terminated PDMS (h-PDMS). The shear modulus was tuned by adding different amounts and different molecular weights of non-reactive trimethyl-terminated PDMS (t-PDMS) to the hydrosilylation mixture. The uniform finish of the soft PDMS surfaces was achieved by tailoring the spin coating speed for the hydrosilylation mixture. The shear modulus of the soft PDMS materials was found to decrease monotonically with the increasing concentration of t-PDMS in the hydrosilylation mixture. The measured shear modulus μ of the soft PDMS materials used in the present study are listed in Table 1. Further details about the fabrication of the soft PDMS materials and quantification of their shear modulus can be found in Beemer et al. [55].

For comparison, the shear modulus values of Aluminum (i.e., representative of the metal-based materials commonly used to make airframes of airplanes) and the hard plastic-based material used to make the 3-D printed airfoil/wing model used for the present study are also listed in Table 1. It can be seen clearly that the shear modulus values of the Aluminum and the hard plastic-based material of the 3D printed airfoil/wing model are significantly higher (i.e., 4–6 orders higher) than those of the soft PDMS materials. Therefore, both Aluminum and the hard plastic-based material used to make the test model can be considered as "rigid materials" when compared with the soft PDMS materials used in the present study.

2.2. Experimental setup used to study the dynamic impacts of water droplets onto soft PDMS surfaces

Since the impingement of supercooled water droplets onto airfoil surfaces is the fundamental mechanism to cause ice accretion over aircraft wing surface, an experimental investigation was conducted in the present study to examine the effects of the surface stiffness on the impinging dynamics of water droplets by comparing the dynamic impacts of water droplets onto the soft PDMS surfaces with that onto the rigid surface of the hard plastic material used to make the airfoil/wing model. Fig. 2 shows the schematic of the experimental setup used to study the dynamic impacts of water droplets. A vertical wind tunnel, which is composed of an air conditioner, a contraction section, a test section, pipe systems and a ducted fan, was used to accelerate the water droplets exhausted out from a droplet generator. As shown in Fig. 2, a ducted fan (JP 70EDF 4s∼6s Lipo), which was powered by a constant voltage power supply unit (Volteq HY30100EX) and a rotational speed controller (Platinum Pro v3 100A), was used to drive the airflow inside the vertical wind tunnel. Water droplets out of the droplet generator with a diameter of 3.0 ± 0.1 mm could be accelerated up to 10.0 m/s before impinging onto the surface of the test plate mounted at the bottom of the vertical wind tunnel. The corresponding weber number of the impinging droplets would be up to 4000 (i.e., $We \approx 4000$), which is in the range pertinent to aircraft inflight icing phenomena (e.g., $We > 1500$) [62,63]. A high-speed camera (Fastcam Mini WX100, PCO) with a macro-lens (50 mm Nikkor 1.8D, Nikon) was used to record the dynamic droplet impacting process. A LED spotlight was used to provide light illumination for the visualization of the droplet impacting process. During the experiments, the sampling rate of the cameras was set at 5000 Hz, and at least 10,000 frames of instantaneous images were recorded for each test cases.

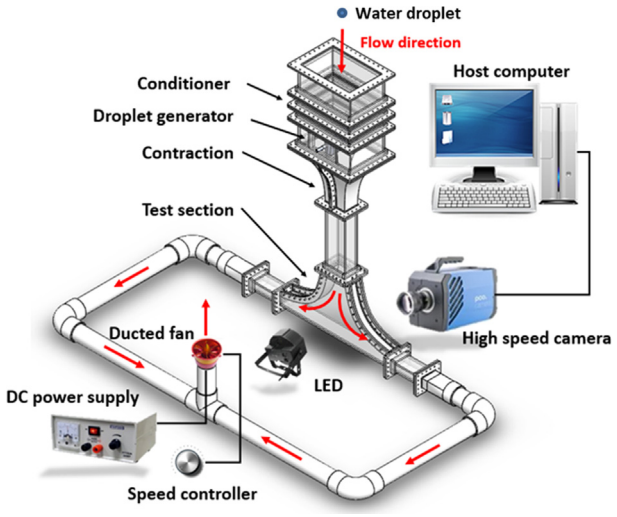

Fig. 2. Experimental setup to study the dynamic impacting of water droplets onto soft PDMS surfaces.

2.3. Airfoil/wing model and the experimental setup used for the impact icing experiment

By depositing the soft PDMS materials onto a NACA 0012 airfoil/wing model, an experimental investigation was also performed to demonstrate the potentials of the soft PDMS materials/surfaces for impact icing mitigation. The impact icing experiments were performed in an Icing Research Tunnel available at Aerospace Engineering Department of Iowa State University (i.e., ISU-IRT). As schematically shown in Fig. 3, the ISU-IRT is a multifunctional icing research tunnel with a test section of 2.0 m in length × 0.4 m in width × 0.4 m in height with four side walls being optically

Table 1
Shear modulus of the soft PDMS materials used in the present study.

Materials	50% t-PDMS	60% t-PDMS	70% t-PDMS	80% t-PDMS	Aluminum	Hard plastic material of 3D printed model
Shear modulus	67 kPa	40 kPa	22 kPa	9.0 kPa	2.5×10^7 kPa	8.0×10^5 kPa

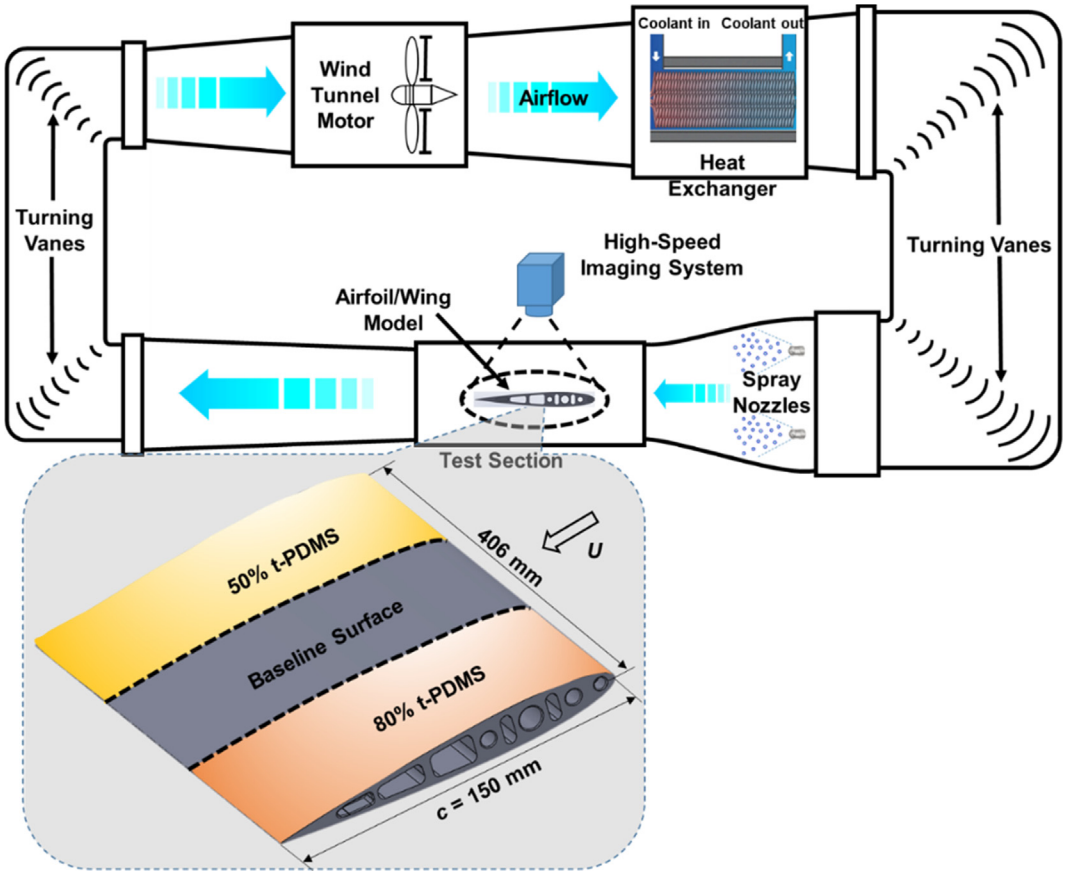

Fig. 3. Schematic of the ISU-IRT and test airfoil/wing model used for the impact icing experiment.

transparent. It has a capacity of generating a maximum wind speed of 60 m/s and an airflow temperature down to −25 °C. An array of 8 pneumatic atomizer/spray nozzles are installed at the entrance of the contraction section of the icing wind tunnel to inject micro-sized water droplets (10–100 μm in size with MVD being ~30 μm) into the airflow. The homogeneity of the icing cloud generated in the ISU-IRT was confirmed by adjusting the settings of the pneumatic atomizer/spray nozzles. By manipulating the water flow rate through the spray nozzles, the liquid water content (*LWC*) in ISU-IRT can be adjusted (i.e., *LWC* ranging from 0.1 g/m^3 to 5.0 g/m^3). In summary, ISU-IRT can be used to simulate atmospheric icing phenomena over a wide range of icing conditions (i.e., from dry *rime* to extremely wet *glaze* ice conditions). In the present study, a typical glaze ice accretion process was simulated in ISU-IRT with the freestream airflow velocity of U_∞ = 40 m/s, liquid water content (*LWC*) of *LWC* = 1.0 g/m^3, and the temperature of T_∞ = −5 °C.

The NACA0012 airfoil/wing model used in the present study has a chord length of c = 150 mm, which spanned the entire width of the test section of ISU-IRT. Supported by a stainless-steel rod, the airfoil/wing model was mounted at its quarter-chord and oriented horizontally across the middle of the test section. The airfoil/wing model was made of a hard plastic-based material and manufactured by using a rapid prototyping machine (i.e., 3-D printing) that builds the 3-D model layer-by-layer with a resolution of about 50 μm. The surface of the airfoil/wing model was wet-sanded by using a series of progressively finer sandpapers (up to 2000 grit) to achieve a very smooth, glossy finish with a characteristic roughness of about 20 μm. Then, a readily available all-weather protective spray-on enamel (Rustoleum, Flat Protective Enamel, white in color) was coated onto the airfoil surface. The surface of the airfoil/wing model treated in such an approach has been found to be hydrophilic, as reported in Waldman et al. [64]. Then, the hydrophobic PDMS gel surfaces with t-PDMS concentration of 50% and 80% were deposited on two sides of airfoil/wing model with a spacing of 50 mm. Thus, as shown schematically in Fig. 3, the airfoil/wing model possessed three distinct zones with different surface characteristics along the spanwise direction (i.e., the uncoated hydrophilic surface with a spanwise length of 50 mm in the middle as the comparison baseline, soft PDMS surfaces with t-PDMS concentration being 50% and 80% on the two ends of the test model).

As shown in Fig. 3, a high-speed imaging system (i.e., PCO Tech, Dimax™ camera with 2000 pixel by 2000 pixel and frame rate of up to 10,000 frames per second) was used to record the dynamic ice accretion processes over the surface of the airfoil/wing model coated with the soft PDMS materials with different shear modulus. The high-speed camera was installed at about 500 mm above the airfoil/wing model with a 60 mm lens (Nikon, 60 mm Nikkor 2.8*D*). The camera was positioned approximately normal to the chord of the airfoil/wing model with a measurement window of 210 × 210 mm^2 (i.e., the resolution of the acquired images being 9.5 pixels/mm). An in-situ calibration procedure as suggested by Soloff et al. [65] was performed to dewarp the captured images before extracting accreted ice features from the acquired images. In the present study, at least 10,000 images were acquired during the impact icing experiment for each test cases.

3. Results and discussions

3.1. Characterization of the surface properties of the soft PDMS materials

In the present study, a series of experiments were conducted to characterize the wettability of the soft PDMS materials with

different shear modulus. At first, by using the similar procedure as that described in Waldman et al. [64], the static contact angles of sessile water droplets placed on the soft PDMS materials were measured. Then, with a similar needle-in-the-sessile-drop method as that described in Korhonen et al. [66], the receding and advancing angles of water droplets (i.e., $\theta_{advancing}$ and $\theta_{receding}$) over the surfaces of the soft PDMS materials were also measured quantitatively. Table 2 summarizes the measured static contact angle θ_{static}, advancing contact angle $\theta_{adv.}$, and receding contact angle $\theta_{rec.}$ along with the corresponding hysteresis $\Delta\theta$ of the soft PDMS materials with different shear modulus (i.e., with the t-PDMS concentration being varied from 50% to 80%). The corresponding values for the original surface of the 3D printed airfoil/wing model (i.e., without applying the soft PDMS materials to cover the airfoil surface) were also listed in the table for comparison.

It is clearly seen that, the measured static contact angle of water droplets sitting on the original surface of the 3D printed airfoil/wing model coated with Enamel (i.e., the baseline surface) was found to be 65° (i.e., $\theta \approx 65°$), indicating the original airfoil surface being hydrophilic before applying the soft PDMS materials to cover the airfoil surface, which is similar as the hydrophilic Aluminum surface of conventional aircraft wings. The measured static contact angles of the water droplets on the soft PDMS surfaces with different shear modulus were found to be almost the same value of 110° (i.e., $\theta \approx 110°$), indicating that the soft PDMS surfaces are hydrophobic with their wettability being almost independent of the shear modulus of the material. It is also found that, while the contact angle hysteresis (i.e., the difference between the advancing and receding contact angles of the water droplets, $\Delta\theta = \theta_{advancing} - \theta_{receding}$) for the baseline airfoil surface was about 55°, the contact angle hysteresis for the soft PDMS materials/surfaces were found to be about 11°, which is also almost independent of the surface shear modulus of the PDMS materials. It should be noted that, the static contact angle of about 110° for PDMS surfaces (i.e., CA $\approx$ 110°) is due to the smooth nature of the material. As suggested by Golovin et al. [68], superhydrophobic PDMS surfaces with CA > 150° can be created by adding roughness textures over the smooth PDMS surfaces.

For a water droplet sitting over a test surface, the droplet would be in motion as an external force is applied onto the droplet (e.g., the shear forces exerted by the incoming airflow for the present study) becoming greater than the capillary force acting on the water droplet. As described in Waldman et al. [64] and Liu et al. [67], the capillary force acting on a moving water droplet over a surface can be estimated with the following equation:

$$F_{capillary} \approx \pi R \gamma_{LG} \left[\sin\left(\frac{\theta_{adv} - \theta_{rec}}{2}\right) \sin\left(\frac{\theta_{adv} + \theta_{rec}}{2}\right) \right] \quad (1)$$

where γ_{LG} is the liquid-gas surface tensions, and R is the spherical cap radius of the water droplet. $\theta_{advancing}$ and $\theta_{receding}$ are the advancing and receding angles of the water droplet, respectively.

Based on the measured receding and advancing angles given in Table 2, the ratio of the capillary forces acting on a water droplet siting on the hydrophilic baseline surface to that of the same droplet on the hydrophobic PDMS surfaces can be estimated based on Eq. (1), which can be expressed as:

$$\frac{F_{cap,\mathrm{PDMS}}}{F_{cap,\mathrm{baseline}}} \approx \frac{\left[\sin\left(\frac{\theta_{adv}-\theta_{rec}}{2}\right)\sin\left(\frac{\theta_{adv}+\theta_{rec}}{2}\right)\right]_{PDMS}}{\left[\sin\left(\frac{\theta_{adv}-\theta_{rec}}{2}\right)\sin\left(\frac{\theta_{adv}+\theta_{rec}}{2}\right)\right]_{\mathrm{baseline}}} \approx 0.2 \quad (2)$$

It reveals clearly that, in comparison with those acting on the water droplets siting on the hydrophilic baseline surface, the capillary forces acting on the water droplets with the same spherical cap radius over the soft PDMS surfaces were found to be much smaller (i.e., becoming only about 1/5). Therefore, only very small external forces are required to overcome the much smaller capillary forces (i.e., being only ~20% in magnitude) to make water droplets to move over the PDMS coated airfoil surface, in comparison with those on the hydrophilic surface of the 3D printed airfoil/wing model before coated with the soft PDMS material. It also suggests that, as driven by the same incoming airflow over the surface of the same airfoil/wing model under the same glaze icing condition to be generated in ISU-IRT, the impinged water droplets/rivulets are expected to run back much faster over the PDMS coated airfoil surfaces than those over the hydrophilic baseline surface, which was confirmed from the measurement results of the ice accretion experiment to be discussed later.

In the present study, the ice adhesion strengths over the surfaces of the soft PDMS materials were also measured by using a similar test rig as that used by Meuler et al. [43]. During the experiments, the temperature of the test surface was maintained at a pre-scribed low temperature (i.e., at $T_w = -10$ °C or $T_w = -5$ °C for the present study). Ten test trials were performed for each test cases, and the mean and standard deviation values of the ice adhesion strength were obtained based on the measurement results. Fig. 4 shows the measured ice adhesion strength of the soft PDMS surfaces/materials as a function of the shear modulus with the temperature of the test surfaces being $T_w = -10$ °C and -5 °C,

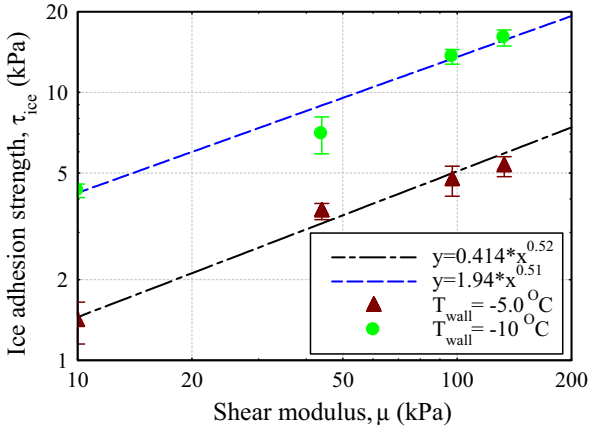

Fig. 4. Measured ice adhesion strength over the soft PDMS surfaces as a function of the material shear modulus.

Table 2
Measurement results of the contact angles over the soft PDMS surfaces.

Compared surface	Static CA θ_{static} (°)	Advancing CA θ_{adv} (°)	Receding CA θ_{rec} (°)	Hysteresis $\Delta\theta = \theta_{adv} - \theta_{rec}$ (°)
Original surface of the 3D printed airfoil model (i.e., baseline surface)	65	105	50	55
50% t-PDMS	110	110	99	11
60% t-PDMS	110	111	99	12
70% t-PDMS	109	110	99	11
80% t-PDMS	109	110	100	10

respectively. It should be noted that, as reported in Liu et al. [67], the ice adhesion strength on the hydrophilic baseline surface (i.e., the original surface of the 3D printed airfoil/wing model coated with Enamel) was found to be about 1400 kPa at $T_w = -10$ °C. At the same low temperature of $T_w = -10$ °C, the ice adhesion strength over the surface of the soft PDMS material with 80% t-PDMS was found to be only about 5.0 kPa, which is significantly smaller than that over the hydrophilic baseline surface (i.e., about two orders of magnitude smaller). It can also be seen that, while the ice adhesion strengths over the soft PDMS surfaces/materials were found to increase monotonically with the shear modulus of the material, the magnitude of the ice adhesion strength increases with the decreasing temperature of the test surface/material.

As described in Kendall [59] and Chaudhury & Kim [60], the relationship between the adhesion shear stress, τ, and the work of adhesion, W_a, can be derived theoretically with an adhesion mechanics model, which is expressed as:

$$\tau \cong \frac{a}{\sqrt{(\alpha a^2 + \beta l^2)}} \left(\frac{W_a \mu}{h}\right)^{\frac{1}{2}} \quad (3)$$

where μ is the shear modulus of the surface material; and h is the thickness of the surface film; a is the size of the rigid stud, l is the distance between the force location and the interface; α and β are the numerical constants, which can be evaluated experimentally. For the test cases of the present study, since the experimental setup for the ice adhesion measurements were kept the same, the measured ice adhesion strength would be proportional to $(W_a\mu/h)^{1/2}$ theoretically. As shown clearly in Fig. 4, the relationship between the measured ice adhesion strengths over the soft PDMS surfaces and the shear modulus of the PDMS materials was found to be fitted reasonably well by using a "Square-Root Law", i.e., $\tau_{ice} \propto \mu^{0.5}$. It indicates that the measurement results of the present study agree reasonably well with the theoretical predictions of the adhesion mechanics model, i.e., $\tau_{ice} \propto \sqrt{W_{adh}\mu/t}$, as described in Kendall [59] and Chaudhur & Kim [60].

3.2. Dynamic impinging process of water droplets onto the surfaces of the soft PDMS materials

As described above, an experimental investigation was conducted to examine the effects of the surface stiffness (i.e., material shear modulus) on the impinging dynamics of water droplets by comparing the dynamic impacting process of water droplets onto soft PDMS surfaces with that onto a rigid surface (i.e., the surface of the hard-plastic material used to make the airfoil/wing model in the present study). It is well known that, Weber number (We), which can be thought of as a measure of the relative importance of the droplet inertia compared to its surface tension, is usually used to characterize droplet impinging process. The Weber number (We) is defines as $We = \rho V^2 D/\sigma$, where ρ is the density of a droplet (kg/m^3); V is the velocity of the droplet (m/s); D is the droplet diameter (m); and σ is the surface tension (N/m). For typical aircraft inflight icing scenario, with the super-cooled water droplets in the cloud being about 10–100 μm and aircraft flying speed being greater than 100 m/s, the corresponding Weber number would be greater than 1500 (i.e., $We > 1500$).

As shown schematically in Fig. 2, a vertical wind tunnel was used in the present study to accelerate the water droplets exhausted from a droplet generator in order to ensure that the droplet impinging experiments were conducted at relatively high Weber numbers (i.e., $We > 1500$) pertinent to aircraft inflight icing phenomena. Fig. 5 shows typical snapshot images to reveal the dynamic process of water droplet impinging onto soft PDMS surfaces at a relatively high Webber number of about 4000 (i.e., $We \approx 4000$). While the droplet impacting experiments were conducted for all the 4 compared PDMS materials with different shear modulus, only the results for the PDMS materials with 50% t-PDMS and 80% t-PDMS concentrations (i.e., the stiffest and the softest cases among the four compared PSMS materials) were given here for conciseness. The snapshot images for the case with the water droplet impinging onto the rigid surface of the hard-plastic material were also given here as the comparison baseline in order to reveal the effects of the surface stiffness on the impinging dynamics of the water droplets more clearly.

As shown clearly in the time sequence of the acquired snapshot images given in Fig. 5(a), after impinging onto the conventional rigid surface (i.e., the surface of the hard-plastic material used to make the airfoil/wing model), the impinged water mass was found to start spreading out rapidly over the rigid surface. After reaching its maximum spreading diameter at the time instant of $t \approx 3.0$ ms, the impinged water mass was found to undergo a receding process with the surface water flowing back to the impinging center, as expected. After several spreading-and-receding cycles, the impinged water mass was finally found to reach a static state and settle down in a formation of "pancake-liked" water film over the impinged rigid surface. Upon droplet impinging onto the rigid surface, only a very small amount of the impinged water mass was found to be splashing out from the rigid surface to form tiny "satellite" droplets along the rim of the out-spreading ring of the impinged waster mass, while majority of the impinged water mass was found to stick firmly on the impinged rigid surface during the entire spreading-and-receding process.

As shown clearly in Fig. 5(b), upon the impingement of the water droplet at the same Weber number level of $We \approx 4000$, the surface of the soft PDMS material with 50% t-PDMS was found to deform dynamically due to the elastic nature of the PDMS material. Induced by the dynamic surface deformations of the elastic PDMS material, the impinged water mass was found to be bounced off from the soft PDMS surface while it was still found to undergo the similar spreading-and-receding process as that over the rigid surface as shown in Fig. 5(a). It implies that, the dynamically deforming surface of the elastic PDMS material behaved like a "trampoline" to bounce off the impinged water mass away from the impacted PDMS surface (i.e., "trampoline effect"). Splashing of the impacted water mass into hundreds of tiny "satellite" droplets was also much more obvious for this test case, in comparison to that with the water droplet impinging onto the rigid surface described above.

Since the shear modulus of the PDMS material with 80% t-PDMS is much smaller than that with 50% t-PDMS (i.e., being only 1/7 in magnitude as listed in Table), the PDMS material with 80% t-PDMS would be much softer in comparison to that with 50% t-PDMS. As revealed from the time sequence of the acquired snapshot images given in Fig. 5(c), the dynamic deformation of the surface of the elastic PDMS material with 80% t-PDMS was found to be become much more significant upon the impingement of the water droplet at the same Weber number level of $We \approx 4000$. Due to the much stronger "trampoline effect" associated with the greater surface deformation for this elastic PDMS material, almost all the impinged water mass was found to be bounced off from the more deformable surface, forming a "bowl-liked" structure, as shown clearly in the snapshots taken at the time instant of $t < 3.0$ ms. As the time goes on, the out-spreading "bowl-liked" water film was found to break up into thousands of tiny droplets subsequently. As a result, upon the impinging of the water droplet onto the softest PDMS material with 80% t-PDMS, the impacted water mass was found to be completely splashed from the impacted elastic PDMS surface with no water mass being sticking onto the impacted surface all the time.

In summary, the findings derived from the droplet impacting experiment reveal clearly that, the impinging dynamics of water droplets would be affected greatly by the stiffness of the impacted

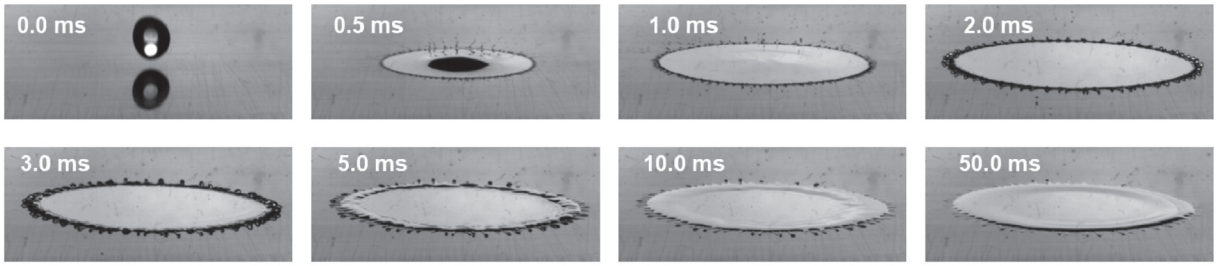

(a) Dynamic impingement of a water droplet onto a conventional rigid surface (i.e., hard-plastic surface)

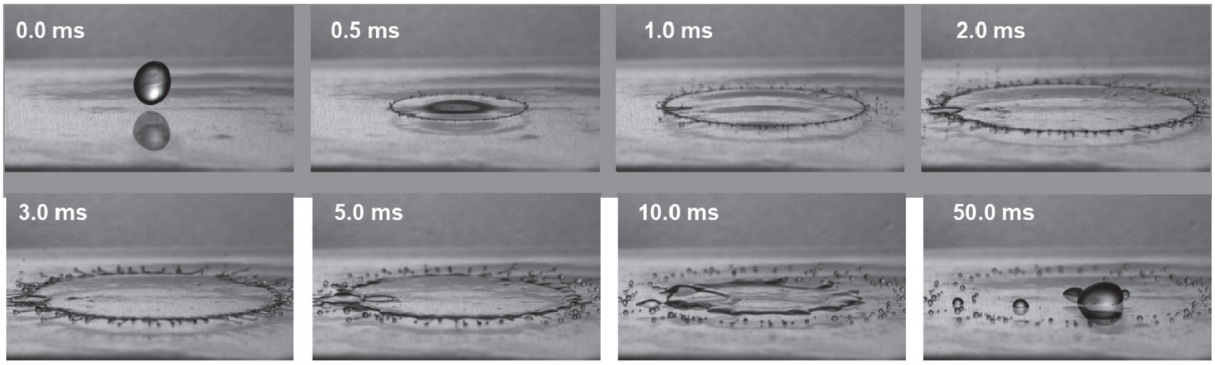

(b) Dynamic impingement of a water droplet onto the stiffest PDMS material with 50% t-PDMS

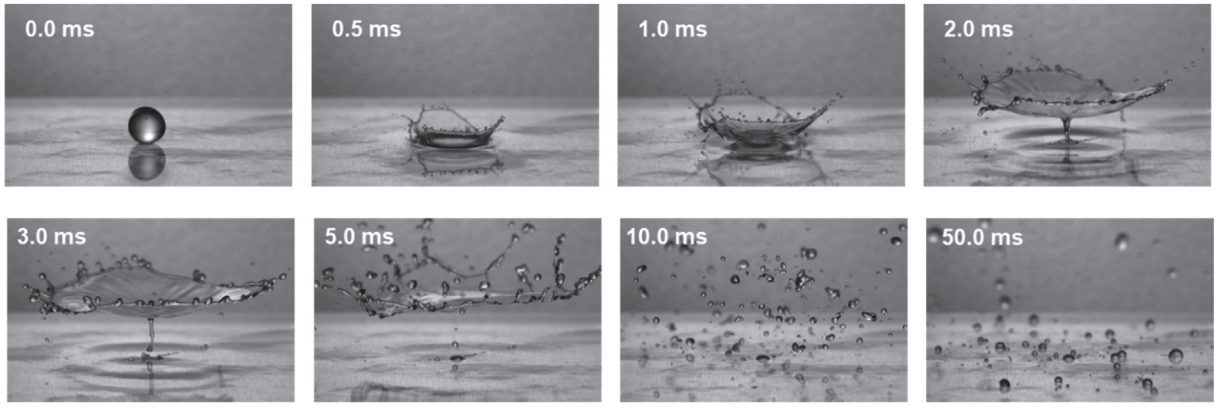

(c) Dynamic impingement of a water droplet onto the surface of the softest PDMS material with 80% t-PDMS

Fig. 5. Time-evolution of the dynamic impinging processes of water droplets onto the conventional rigid surface and soft PDMS surfaces at a relatively high Weber number of $We \approx 4000$.

surface. Upon the impingement of water droplets, the surfaces of the soft PDMS materials were found to be deformed dynamically. Induced by the dynamic deformations over the soft surfaces, the elastic PDMS materials were found to act as "trampolines" to bounce off the impacted water mass away from the impacted surface. Since the "trampoline effect" of the soft PDMS materials was found to be able to effectively bounce off the impinging water droplets from the surfaces, it causes a substantial reduction of the wetted area over the impacted surfaces. By taking advantage of the "trampoline effect" of the soft PDMS materials, a new mechanism for impact icing mitigation will be discussed in further detail in the next section.

3.3. Anti-icing performance of the soft PDMS surface

As described above, an explorative study was also conducted in the present study to demonstrate the feasibility of using the soft PDMS materials/surfaces to mitigate the impact icing pertinent to aircraft icing phenomena. To perform the impact icing mitigation experiment, ISU-IRT was operated at a pre-scribed frozen-cold temperature level (e.g., $T_\infty = -5$ °C for the present study) for at least 20 min under a dry airflow condition (i.e., without turning on the water spray system of ISU-IRT) to ensure that ISU-IRT reached at a thermal steady state. After switching on the water spray system, the supper-cooled water droplets carried by the frozen-cold airflow would impinge onto the surface of the airfoil/wing model (i.e., mainly within the direct impact zone near the airfoil leading edge [69]) to start ice accreting process. In the present study, with the icing test conditions of the freestream airflow velocity being $U_\infty = 40$ m/s, airflow temperature of $T_\infty = -5$ °C and the liquid water content level (*LWC*) in the airflow being 1.0 g/m^3, (i.e., *LWC* = 1.0 g/m^3), the ice accretion over the surfaces of the airfoil/wing model is expected to be of a typical glaze icing process (i.e., with obvious surface water runback process and formation of transparent ice structures), as described in Waldman and Hu [7].

Fig. 6 shows the typical snapshot images to reveal the dynamic ice accretion processes over the airfoil/wing surfaces with different surface properties (i.e., the soft surface with 50% t-PDMS at the left, the rigid baseline surface in the middle, and softest surface with 80% t-PDMS at the right). As revealed clearly from the acquired snapshot images given in the middle column, i.e., Fig. 6(B), after the super-cooled water droplets impinged onto the rigid baseline airfoil surface, a typical glaze ice accreting process was observed with obvious surface water runback to form rivulet-shaped ice structures over the airfoil surface. This can be explained by the facts that, under such a wet glaze icing condition (i.e., with U_∞ = 40 m/s, T_∞ = −5 °C, and LWC = 1.0 g/m^3), upon the dynamic impacting of a large number of super-cooled water droplets onto the airfoil surface, a tremendous latent heat of fusion would be released associated with the solidification of the impacted super-cooled water mass. As described in Liu et al. [69], since the heat transfer process over the surface of the airfoil/wing model under such a wet icing condition would not be able to remove/dissipate all the released latent heat of fusion immediately, only a portion of the impinged super-cooled water droplets would be solidified and turn into solid ice upon impact, while the rest of the impinged water mass would stay in liquid state and was able to flow freely over the airfoil surface. Driven by the airflow over the airfoil surface, the unfrozen surface water would run back along the airfoil surface in the form of rivulet flows [70], which would be frozen into ice eventually at the further downstream locations, i.e., beyond the direct impact zone of the super-cooled water droplets, as shown clearly in Fig. 6(B).

It can also be seen clearly that, in comparison with that over the rigid baseline surface, the ice accreted over the airfoil/wing surfaces covered with soft PDMS materials was found to be mitigated greatly, i.e., the areas with ice accretion over the soft PDMS covered airfoil/wing surfaces (i.e., for both the airfoil surfaces covered with 50% t-PDMS on the left and 80% t-PDMS on the right) were found to be reduced significantly. The reduced ice accretion over the PDMS covered airfoil/wing surfaces are believed to be caused by following reasons: As revealed clearly from the results of the droplet impacting experiments given in Fig. 5, with the super-cooled water droplets impinging onto the rigid airfoil surface (i.e., baseline surface), the impacted water mass would spread out over the airfoil surface to form a thin water film. The impacted water mass would stay on the airfoil surface, and subsequently freeze into ice over the airfoil surface. However, as the super-cooled water droplets impinging onto the airfoil surfaces covered with soft PDMS materials, due to the elastic nature of the soft PDMS materials, i.e., "trampoline effect" described above, majority of the impacted water mass would be bounced off from the soft PDMS surfaces, as shown clearly in Fig. 5. As a result, even though the airfoil/wing model was exposed into the same incoming airflow under the same glaze icing conditions, the collected water mass over the PDMS covered airfoil surfaces would be much less than that over the rigid airfoil surface (i.e., the baseline case). Therefore, the total amount of the ice that can be accreted over the PMDS covered airfoil surfaces would be much less, in compassion with that over the baseline surface. Furthermore, under the glaze icing condition of the present study, since the impacted water mass over the airfoil surface would not be completely frozen immediately, the unfrozen water mass would run back over the airfoil surface, as driven by the boundary layer airflow over the airfoil surface. As described in Section 3.1, for the same droplet/rivulet flows over the airfoil surfaces, since the capillary forces acting on droplet/rivulet flows over the hydrophobic PDMS surfaces would be much smaller i.e., becoming only ~20% in magnitude of that over the rigid, hydrophilic baseline surface, the runback speed of the water droplets/rivulets were expected to be much faster over the PDMS coated airfoil surface, in comparison with those over the hydrophilic baseline surface. As a result, a portion of the runback surface water would be able to flow out of the airfoil surface before being frozen into solid ice. Even for the scenario with ice having already been accreted over the airfoil surface, due to the much smaller ice adhesion strength over the soft PDMS surfaces than that over the baseline surface (i.e., ice adhesion strength being <10 kPa over the soft PDMS surfaces as shown in Fig. 4 vs. that being >1000 kPa over the rigid baseline surface at T_{wall} = −5 °C as reported by Liu et al. [67]), the aerodynamic stress from the airflow over the airfoil/wing surface would more likely sweep away the ice accreted on the airfoil surface covered with the icephobic PDMS materials, in comparison with the ice accreted on the baseline surface of the airfoil/wing model.

By comparing the two test cases of the airfoil surfaces covered by PDMS materials with different shear modulus (i.e., 50% t-PDMS surface *vs.* 80% t-PDMS surface), the ice accretion area over the airfoil surface covered by the PDMS material with 80% t-PDMS

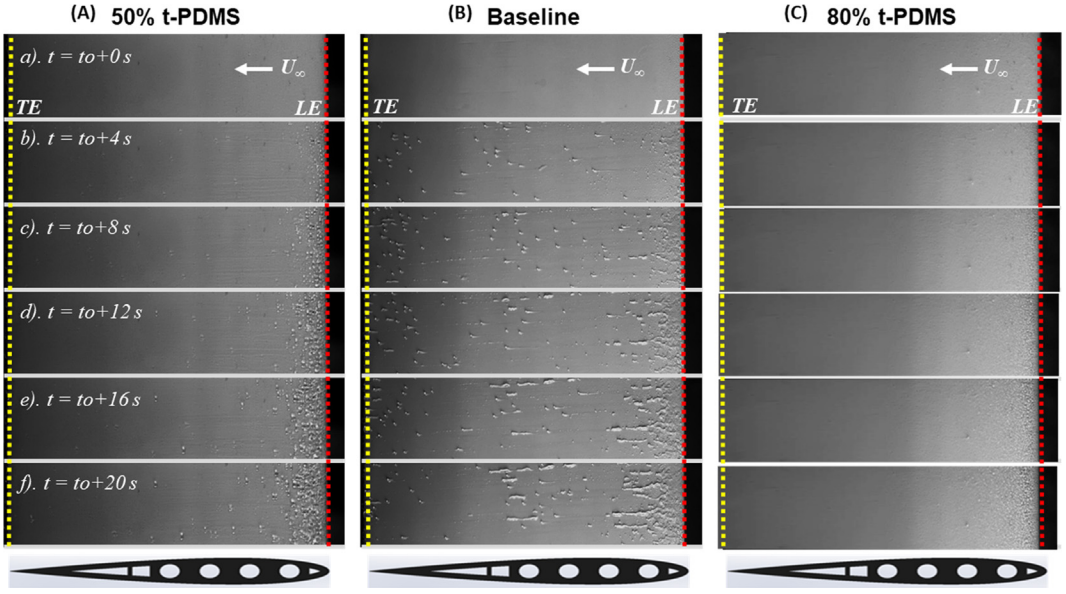

Fig. 6. Typical snapshots to reveal the dynamic ice accretion process over the surface of the airfoil/wing model under the glaze icing condition of U_∞ = 40 m/s, T_∞ = −5 °C and LWC = 1.0 g/m^3.

(i.e., the case with smaller shear modulus) was found to be obviously less than that over the airfoil surface coated with 50% t-PDMS. This is believed to be caused by the fact that the impinging water droplets would be more easily bounced off from the softer PDMS surface (i.e., 80% t-PDMS surface), i.e., due to the more obvious "trampoline effect" of the softer PDMS surface, as described above.

It should also be noted that, even though the present study demonstrated clearly that ice accretion over an airfoil/wing surface can be mitigated significantly by applying soft PDMS materials to cover/coat the airfoil surfaces, ice was still found to form near the leading edge of the PDMS coated airfoil/wing surfaces in the vicinity of the airfoil stagnation line. This highlights one of the major challenges facing hydro-/ice-phobic coating strategies. The hydro-/ice-phobic coatings produce low adhesion forces between the airfoil surface and water and/or ice and rely on aerodynamic stresses acting tangentially to the surfaces to remove the water/ice accretion. Such approaches would break down at the airfoil stagnation line because the shear stress near the airfoil stagnation line would be very small or completely vanish. Further exacerbating the problem is that the water collection efficiency is a maximum at the stagnation line. Once ice started to accrete along the stagnation line of the airfoil/wing surface, the super-cooled water droplets carried by the incoming airflow would impact directly onto the surface of the accreted ice, instead of the PDMS coated airfoil surface, to cause further ice accretion. The experimental results given above illustrate clearly how conventional coatings that are effectively hydro- or/and ice-phobic at nominal conditions may not perform well under impact icing conditions pertinent to aircraft icing phenomena.

4. Conclusion

An experimental study was conducted to evaluate the anti-/de-icing performance of soft PDMS materials and to explore their application potentials for aircraft icing mitigation. A class of soft PDMS materials with adjustable shear modulus were fabricated by adding different concentrations of non-reactive trimethyl-terminated PDMS (t-PDMS) into the hydrosilylation mixture of vinyl-terminated PDMS (v-PDMS) and hydride-terminated PDMS (h-PDMS). The material properties of the soft PDMS materials were characterized in terms of static contact angles, dynamic contact angles of water droplets, and ice adhesion strength over the surfaces of the PDMS materials at different frozen temperatures. An experimental investigation was conducted to examine the effects of the surface stiffness (i.e., material shear modulus) on the impinging dynamics of water droplets by comparing the dynamic process of water droplets impacting onto soft PDMS surfaces with that onto a conventional rigid surface (i.e., the surface of the hard-plastic material used to make the airfoil/wing model in the present study as the comparison baseline) at relatively high weber numbers pertinent to aircraft inflight icing phenomena. By applying the soft PDMS materials to coat/cover the surface of a NACA 0012 airfoil/wing model, an explorative study was performed in an Icing Research Tunnel available at Iowa State University (i.e., ISU-IRT in short) to demonstrate the feasibility of using the soft PDMS surface/materials to mitigate impact icing process pertinent to aircraft inflight icing phenomena.

It was found that, while the soft PDMS materials were hydrophobic as demonstrated by the measured contact angle being greater than 90° (i.e., measured $\theta \approx 110°$), the hydrophobicity of the PDMS materials was found to be almost unchanged with the varying shear modulus. The measured contact angle hysteresis of the PDMS materials was also found to be only about 11° (i.e., $\Delta\theta = \theta_{adv} - \theta_{rec} \approx 11°$). Corresponding to larger contact angle and the much smaller contact angle hysteresis of the soft PDMS materials, the capillary forces acting on the water droplets sited on the surfaces of the soft PDMS materials would become much smaller (i.e., becoming only of 20% in magnitude) in comparison with those acting on the water droplets siting on the rigid baseline surface with the same droplet wet area. It implies that, only a much smaller external force would be needed to overcome the smaller capillary forces in order to drive the water droplets to move over the PDMS surfaces. The ice adhesion strength of the soft PDMS surfaces was also found to be significantly smaller than that of the hydrophilic surface (i.e., about two orders of magnitude smaller), which can promise a great anti-/de-icing performance of the surfaces coated with the soft PDMS materials.

The impinging dynamics of water droplets was found to be affected greatly by the stiffness of the impacted surface. Upon the impingement of water droplets, the surfaces of the soft PDMS materials were found to be deformed dynamically. Due to the elastic nature of the PDMS materials, the soft PDMS materials were found to act as "trampolines" to bounce off the impacted water mass away from the impacted surface. Such a "trampoline effect" of the soft PDMS materials was found to be able to effectively keep the impinged water droplet away from the impacted surface, therefore, substantially reduce the wetted area during the droplet impinging process, which provides a new mechanism for impact icing mitigation.

By comparing the dynamic impact icing processes over different surfaces (50% t-PDMS surface, hydrophilic baseline surface, and 80% t-PDMS surface) of the same NACA 0012 airfoil/wing model under a typical glaze icing condition, it was demonstrated clearly that the impact icing would be mitigated greatly by covering/coating the airfoil surface with the soft PDMS materials. The much less ice accretion over the soft PDMS covered airfoil/wing surfaces are believed to be due to the following three reasons: (1) The "trampoline effect" of the soft PDMS materials would effectively bounce off the impinged super-cooled water droplets away from the airfoil surface, therefore, substantially reduce the total amount of the impacted water mass sticking on the airfoil surface; (2) The much faster runback speed of the surface water droplets/rivulets over the PDMS surfaces associated with the much smaller capillary forces acting on the water droplets/rivulets, in comparison to those acting the water droplets/rivulets over the hydrophilic baseline surface, would enable the unfrozen surface water to shed off quickly from the airfoil/wing model before being frozen into ice; (3) The much smaller ice adhesion force over the PDMS surfaces (i.e., about 2 orders of magnitude smaller in comparison to the baseline surface) would enable the aerodynamic stress from the airflow over the airfoil/wing surface more likely to sweep away the ice structures accreted on the airfoil surface covered with soft PDMS materials, in comparison with those accreted on the baseline surface of the airfoil/wing model.

Acknowledgments

The authors want to thank Mr. Prashanth Sagar, Mr. James Benson and Mr. Andrew Jordan of Iowa State University for their help in operating ISU Icing Research Tunnel (ISU-IRT) Facility. The research work is partially supported by Iowa Space Grant Consortium (ISGC) Base Program for Aircraft Icing Studies, National Aeronautics and Space Administration (NASA) with the grant numbers of NNX16AN21A and NNX12C21A, and National Science Foundation (NSF) under award numbers of CBET1064196 and CBET-1435590.

References

[1] M. Bragg, G. Gregorek, J. Lee, Airfoil aerodynamics in icing conditions, J. Aircr. 23 (1986) 76–81.

[2] K. Ueno, M. Farzaneh, Linear stability analysis of ice growth under supercooled water film driven by a laminar airflow, Phys. Fluids 23 (2011) 42103, https://doi.org/10.1063/1.3575605.
[3] G. Fortin, J.-L. Laforte, A. Ilinca, Heat and mass transfer during ice accretion on aircraft wings with an improved roughness model, Int. J. Therm. Sci. 45 (2006) 595–606, https://doi.org/10.1016/j.ijthermalsci.2005.07.006.
[4] Y. Liu, L.J. Bond, H. Hu, Ultrasonic-attenuation-based technique for ice characterization pertinent to aircraft icing phenomena, AIAA J. 55 (2017) 1–8, https://doi.org/10.2514/1.J055500.
[5] Y. Liu, W.-L. Chen, L.J. Bond, H. Hu, An experimental study on the characteristics of wind-driven surface water film flows by using a multi-transducer ultrasonic pulse-echo technique, Phys. Fluids 29 (2017) 12102, https://doi.org/10.1063/1.4973398.
[6] S. Lee, E. Loth, Simulation of icing on a cascade of stator blades, J. Propuls. Power. 24 (2008) 1309–1316, https://doi.org/10.2514/1.37810.
[7] R.M. Waldman, H. Hu, High-speed imaging to quantify transient ice accretion process over an airfoil, J. Aircr. 53 (2015) 369–377, https://doi.org/10.2514/1.C033367.
[8] Y. Liu, L. Li, Z. Ning, W. Tian, H. Hu, Experimental investigation on the dynamic icing process over a rotating propeller model, J. Propuls. Power. (2018) 1–15, https://doi.org/10.2514/1.B36748.
[9] R. Kent, D. Andersen, Canadian water quality guidelines for glycols – an ecotoxicological review of glycols and associated aircraft anti-icing and deicing fluids, Environ. Toxicol. 14 (5) (1999) 481–522.
[10] S.K. Thomas, R.P. Cassoni, C.D. MacArthur, Aircraft anti-icing and de-icing techniques and modeling, J. Aircr. 33 (1996) 841–854, https://doi.org/10.2514/3.47027.
[11] J. Lv, Y. Song, L. Jiang, J. Wang, Bio-inspired strategies for anti-icing, ACS Nano 8 (2014) 3152–3169, https://doi.org/10.1021/nn406522n.
[12] C. Antonini, M. Innocenti, T. Horn, M. Marengo, A. Amirfazli, Understanding the effect of superhydrophobic coatings on energy reduction in anti-icing systems, Cold Reg. Sci. Technol. 67 (2011) 58–67, https://doi.org/10.1016/j.coldregions.2011.02.006.
[13] L. Cao, A.K. Jones, V.K. Sikka, J. Wu, D. Gao, Anti-icing superhydrophobic coatings, Langmuir 25 (2009) 12444–12448, https://doi.org/10.1021/la902882b.
[14] L. Boinovich, A. Emelyanenko, Anti-icing potential of superhydrophobic coatings, Mendeleev Commun. 23 (2013) 3–10.
[15] L. Mazzola, Aeronautical livery coating with icephobic property, Surf. Eng. 32 (2016) 733–744, https://doi.org/10.1080/02670844.2015.1121319.
[16] I. Catapano, F. Soldovieri, L. Mazzola, C. Toscano, THz imaging as a method to detect defects of aeronautical coatings, J. Infrared Millimeter Terahertz Waves 38 (2017) 1264–1277, https://doi.org/10.1007/s10762-017-0404-z.
[17] L. Mazzola, L. Coriand, N. Felde, G. Bruno, B. Galasso, V. Quaranta, F. Albano, A. Auletta, Development and technological characterization of multi-functional aeronautical coating from lab-scale to the relevant environment, J. Aeronaut. Aerosp. Eng. 6 (2017) 1–16, https://doi.org/10.4172/2168-9792.1000182.
[18] H. Vahabi, W. Wang, K.C. Popat, G. Kwon, T.B. Holland, A.K. Kota, Metallic superhydrophobic surfaces via thermal sensitization, Appl. Phys. Lett. 110 (2017) 251602, https://doi.org/10.1063/1.4989577.
[19] S. Movafaghi, W. Wang, A. Metzger, D.D. Williams, J.D. Williams, A.K. Kota, Tunable superomniphobic surfaces for sorting droplets by surface tension 16 (2016) 3204–3209, https://doi.org/10.1039/C6LC00673F.
[20] A. Pendurthi, S. Movafaghi, W. Wang, S. Shadman, A.P. Yalin, A.K. Kota, Fabrication of nanostructured omniphobic and superomniphobic surfaces with inexpensive CO_2 laser engraver, ACS Appl. Mater. Interfaces 9 (2017) 25656–25661, https://doi.org/10.1021/acsami.7b06924.
[21] W. Wang, J. Salazar, H. Vahabi, A. Joshi-Imre, W.E. Voit, A.K. Kota, Metamorphic superomniphobic surfaces, Adv. Mater. 29 (2017) 1700295–n/a. http://doi.org/10.1002/adma.201700295.
[22] H. Vahabi, W. Wang, S. Movafaghi, A.K. Kota, Free-standing, flexible, superomniphobic films, ACS Appl. Mater. Interfaces 8 (2016) 21962–21967, https://doi.org/10.1021/acsami.6b06333.
[23] W. Wang, K. Lockwood, L.M.L. Boyd, M.D. Davidson, S. Movafaghi, H. Vahabi, S. R. Khetani, A.K. Kota, Superhydrophobic coatings with edible materials, ACS Appl. Mater. Interfaces 8 (2016) 18664–18668, https://doi.org/10.1021/acsami.6b06958.
[24] P. Tourkine, M. Le Merrer, D. Quéré, Delayed freezing on water repellent materials, Langmuir 25 (2009) 7214–7216, https://doi.org/10.1021/la900929u.
[25] L. Mishchenko, B. Hatton, V. Bahadur, Design of ice-free nanostructured surfaces based on repulsion of impacting water droplets, ACS Nano 4 (12) (2010) 7699–7707.
[26] K. Varanasi, T. Deng, J. Smith, Frost formation and ice adhesion on superhydrophobic surfaces, Appl. Phys. Lett. 97 (2010) 8234102.
[27] T. Maitra, M.K. Tiwari, C. Antonini, P. Schoch, S. Jung, P. Eberle, D. Poulikakos, On the nanoengineering of superhydrophobic and impalement resistant surface textures below the freezing temperature, Nano Lett. 14 (2014) 172–182, https://doi.org/10.1021/nl4037092.
[28] S. Jung, M. Dorrestijn, D. Raps, A. Das, C.M. Megaridis, D. Poulikakos, Are Superhydrophobic surfaces best for icephobicity?, Langmuir 27 (2011) 3059–3066, https://doiorg/10.1021/la104762g.
[29] V. Hejazi, K. Sobolev, M. Nosonovsky, P.K. Rohatgi, From superhydrophobicity to icephobicity: forces and interaction analysis, Sci. Rep. 3 (2013) 70–71, https://doi.org/10.1038/srep02194.
[30] J. Chen, J. Liu, M. He, K. Li, D. Cui, Q. Zhang, X. Zeng, Y. Zhang, J. Wang, Y. Song, Superhydrophobic surfaces cannot reduce ice adhesion, Appl. Phys. Lett. 101 (2012) 111603, https://doi.org/10.1063/1.4752436.
[31] M. Nosonovsky, V. Hejazi, Why superhydrophobic surfaces are not always icephobic, ACS Nano 6 (2012) 8488–8491, https://doi.org/10.1021/nn302138r.
[32] C. Dorrer, J. Rühe, Some thoughts on superhydrophobic wetting, Soft Matter 5 (2009) 51, https://doi.org/10.1039/b811945g.
[33] A. Lafuma, D. Quéré, Superhydrophobic states, Nat. Mater. 2 (2003) 457–460, https://doi.org/10.1038/nmat924.
[34] C. Antonini, F. Villa, M. Marengo, Oblique impacts of water drops onto hydrophobic and superhydrophobic surfaces: outcomes, timing, and rebound maps, Exp. Fluids 55 (2014) 1713, https://doi.org/10.1007/s00348-014-1713-9.
[35] S.A. Kulinich, M. Farzaneh, How wetting hysteresis influences ice adhesion strength on superhydrophobic surfaces, Langmuir 25 (2009) 8854–8856, https://doi.org/10.1021/la901439c.
[36] A. Meuler, G. McKinley, R. Cohen, Exploiting topographical texture to impart icephobicity, ACS Nano 4 (2010) 7048–7052.
[37] X. Yao, Y. Song, L. Jiang, Applications of bio-inspired special wettable surfaces, Adv. Mater. 23 (2011) 719–734.
[38] T. Sun, L. Feng, X. Gao, L. Jiang, Bioinspired surfaces with special wettability, Acc. Chem. Res. 38 (2006) 644–652.
[39] A. Cassie, S. Baxter, Wettability of porous surfaces, Trans. Faraday Soc. 40 (1944) 1905–1971.
[40] R.N. Wenzel, Resistance of solid surfaces to wetting by water, Ind. Eng. Chem. 28 (1936) 988–994, https://doi.org/10.1021/ie50320a024.
[41] M.A. Sarshar, C. Swarctz, S. Hunter, J. Simpson, C.-H. Choi, Effects of contact angle hysteresis on ice adhesion and growth on superhydrophobic surfaces under dynamic flow conditions, Colloid Polym. Sci. 291 (2013) 427–435, https://doi.org/10.1007/s00396-012-2753-4.
[42] K.K.K. Varanasi, T. Deng, J.D. Smith, M. Hsu, N. Bhate, Frost formation and ice adhesion on superhydrophobic surfaces, Appl. Phys. Lett. 97 (2010) 23–26, https://doi.org/10.1063/1.3524513.
[43] A.J. Meuler, J.D. Smith, K.K. Varanasi, J.M. Mabry, G.H. McKinley, R.E. Cohen, Relationships between water wettability and ice adhesion, ACS Appl. Mater. Interfaces 2 (2010) 3100–3110, https://doi.org/10.1021/am1006035.
[44] J. Soltis, J. Palacios, T. Eden, D. Wolfe, Ice adhesion mechanisms of erosion-resistant coatings, AIAA J. 53 (2015) 654–662, https://doi.org/10.2514/1.J053208.
[45] Y.H. Yeong, E. Loth, J. Sokhey, A. Lambourne, Ice adhesion strength on hydrophobic and superhydrophobic coatings, in: 6th AIAA Atmos. Sp. Environ. Conf., 2014. http://doi.org/10.2514/6.2014-2063.
[46] H. Baker, W.D. Bascom, C. Singleterry, The adhesion of ice to lubricated surfaces, J. Colloid Sci. 17 (1962) 477–491, https://doi.org/10.1016/0095-8522(62)90057-0.
[47] H. Baker, R. Bolster, Factors Affecting the Icing Resistance of Lubricants for Aircraft Ordnance, 1965.
[48] T. Ford, O. Nichols, Adhesion-shear strength of ice frozen to clean and lubricated surfaces, 1962.
[49] T. Ford, O. Nichols, Shear Characteristics of Ice in Bulk, at Ice/Solid Interfaces, and at Ice/Lubricant/Solid Interfaces in a Laboratory Device, Defense Technical Information Center, Ft. Belvoir, 1961.
[50] P. Kim, T.-S. Wong, J. Alvarenga, M.J. Kreder, W.E. Adorno-Martinez, J. Aizenberg, Liquid-infused nanostructured surfaces with extreme anti-ice and anti-frost performance, ACS Nano 6 (2012) 6569–6577, https://doi.org/10.1021/nn302310q.
[51] T.-S. Wong, S.H. Kang, S.K.Y. Tang, E.J. Smythe, B.D. Hatton, A. Grinthal, J. Aizenberg, Bioinspired self-repairing slippery surfaces with pressure-stable omniphobicity, Nature 477 (2011) 443–447, https://doi.org/10.1038/nature10447.
[52] N. Rungraeng, S.H. Yoon, Y. Li, S. Jun, Development of a self-slippery liquid-infused porous surface (SLIPS) coating using carbon nanotube composite for repelling food debris and microbial biofilms, Trans. ASABE 58 (2015) 861–867, https://doi.org/10.13031/trans.58.10939.
[53] H.A. Stone, Ice-phobic surfaces that are wet, ACS Nano 6 (2012) 6536–6540, https://doi.org/10.1021/nn303372q.
[54] H. Sojoudi, M. Wang, N.D. Boscher, G.H. McKinley, K.K. Gleason, Z.Z. Yang, G.H. McKinley, K.K. Gleason, F. Liu, M.L. Hu, S.R. Hunter, J.A. Haynes, K.K. Gleason, Durable and scalable icephobic surfaces: similarities and distinctions from superhydrophobic surfaces, Soft Matter 12 (2016) 1938–1963, https://doi.org/10.1039/C5SM02295A.
[55] D.L. Beemer, W. Wang, A.K. Kota, M. Doi, F. Brochard-Wyart, A. Tuteja, J. Aizenberg, J. Wang, Y. Song, L. Jiang, Durable gels with ultra-low adhesion to ice, J. Mater. Chem. A 4 (2016) 18253–18258, https://doi.org/10.1039/c6ta07262c.
[56] J. Chen, R. Dou, D. Cui, Q. Zhang, Y. Zhang, F. Xu, X. Zhou, J. Wang, Y. Song, L. Jiang, Robust prototypical anti-icing coatings with a self-lubricating liquid water layer between ice and substrate, ACS Appl. Mater. Interfaces 5 (2013), https://doi.org/10.1021/am401004t, 130510105547001.
[57] R. Dou, J. Chen, Y. Zhang, X. Wang, D. Cui, Y. Song, L. Jiang, J. Wang, Anti-icing coating with an aqueous lubricating layer, ACS Appl. Mater. Interfaces 6 (2014) 6998–7003, https://doi.org/10.1021/am501252u.
[58] A.A. Griffith, The phenomena of rupture and flow in solids, Philos. Trans. R. Soc. A Math. Phys. Eng. Sci. 221 (1921) 163–198, https://doi.org/10.1098/rsta.1921.0006.

[59] K. Kendall, The adhesion and surface energy of elastic solids, J. Phys. D Appl. Phys. 4 (1971) 320, https://doi.org/10.1088/0022-3727/4/8/320.
[60] M.K. Chaudhury, K.H. Kim, Shear-induced adhesive failure of a rigid slab in contact with a thin confined film, Eur. Phys. J. E 23 (2007) 175–183, https://doi.org/10.1140/epje/i2007-10171-x.
[61] C. Heo, H. Park, Y.-T. Kim, E. Baeg, Y.H. Kim, S.-G. Kim, M. Suh, A soft, transparent, freely accessible cranial window for chronic imaging and electrophysiology, Sci. Rep. 6 (2016) 27818, https://doi.org/10.1038/srep27818.
[62] M.K. Politovich, Aircraft icing caused by large supercooled droplets, J. Appl. Meteorol. 28 (1989) 856–868, https://doi.org/10.1175/1520-0450(1989)028<0856:AICBLS>2.0.CO;2.
[63] T. Cebeci, F. Kafyeke, Aircraft icing, Annu. Rev. Fluid Mech. 35 (2003) 11–21.
[64] R.M. Waldman, H. Li, H. Hu, An experimental investigation on the effects of surface wettability on water runback and ice accretion over an airfoil surface, in: 8th AIAA Atmos. Sp. Environ. Conf., American Institute of Aeronautics and Astronautics, Virginia, 2016. http://doi.org/10.2514/6.2016-3139.
[65] S.M. Soloff, R.J. Adrian, Z.-C. Liu, Distortion compensation for generalized stereoscopic particle image velocimetry, Meas. Sci. Technol. 8 (1997) 1441–1454, https://doi.org/10.1088/0957-0233/8/12/008.
[66] J.T. Korhonen, T. Huhtamäki, O. Ikkala, R.H.A. Ras, Reliable measurement of the receding contact angle, Langmuir 29 (2013) 3858–3863, https://doi.org/10.1021/la400009m.
[67] Y. Liu, L. Li, H. Li, H. Hu, An experimental study of surface wettability effects on dynamic ice accretion process over an UAS propeller model, Aerosp. Sci. Technol. 73 (2018) 164–172, https://doi.org/10.1016/j.ast.2017.12.003.
[68] K. Golovin, S.P.R. Kobaku, D.H. Lee, E.T. DiLoreto, J.M. Mabry, A. Tuteja, Designing durable icephobic surfaces, Sci. Adv. 2 (2016), https://doi.org/10.1126/sciadv.1501496, e1501496–e1501496.
[69] Y. Liu, H. Hu, An experimental investigation on the unsteady heat transfer process over an ice accreting airfoil surface, Int. J. Heat Mass Transf. 122 (2018) 707–718, https://doi.org/10.1016/j.ijheatmasstransfer.2018.02.023.
[70] K. Zhang, T. Wei, H. Hu, An experimental investigation on the surface water transport process over an airfoil by using a digital image projection technique, Exp. Fluids 56 (2015) 1–16, https://doi.org/10.1007/s00348-015-2046-z.